Supporting Information

Highly reversible Li-ion full batteries using Mg-doped Li-rich $Li_{1.2}Ni_{0.28}Mn_{0.468}Mg_{0.052}O_2$ cathode and carbon-decorated Mn_3O_4 anode with hierarchical microsphere structures

By *Jong Guk Kim,[a†] Yuseong Noh,[b††] and Youngmin Kim*[c]*

[a]Research Center for Materials Analysis, Korea Basic Science Institute (KBSI), 169-148 Gwahak-ro, Yuseong-gu, Daejeon 34133, Republic of Korea

[b]Department of Chemical Engineering, Pohang University of Science and Technology (POSTECH), 77 Cheongam-Ro, Nam-gu, Pohang, Gyeongbuk 37673, Republic of Korea

[c]Chemical & Process Technology Division, Korea Research Institute of Chemical Technology (KRICT), 141 Gajeong-ro, Yuseong-gu, Daejeon 34114, Republic of Korea

†Present Addresses: Dongwon Systems, 68, Mabang-ro, Seocho-gu, Seoul, Republic of Korea

††Present Addresses: Samsung Electronics, Samsungjeonja-ro, Hwaseong-si, Gyeonggi-do 18448, Republic of Korea

* Corresponding Author: Tel: +82-42-610-8576,

E-mail: ykim@krict.re.kr

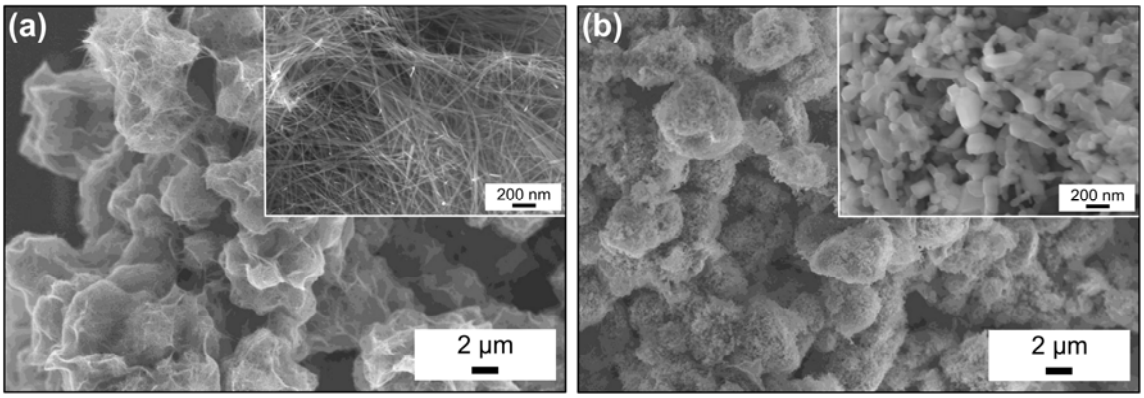

Fig. S1 (a and b) Typical SEM images of the (a) MnO_2 and (b) LLNMO MSs.

Table S1 Crystallographic data of the LLNMO@Mg and LLNMO MSs.

Samples	**Lattice parameters**			***I(003)/I(104)***
	***a* (Å)**	***c* (Å)**	***V* (Å^3)**	
LLNMO@Mg MSs	2.8580	14.2560	100.8446	1.39
LLNMO MSs	2.8560	14.2460	100.6329	1.25

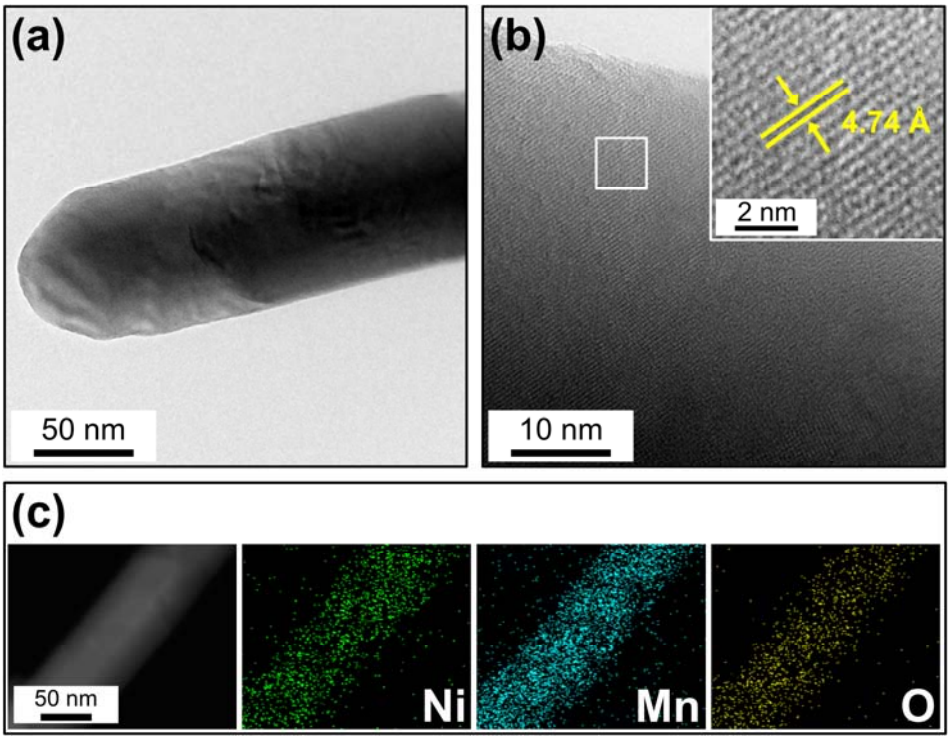

Fig. S2 (a) TEM and (b) HRTEM image of the LLNMO MSs. (c) Dark-field TEM image of LLNMO MSs and corresponding elemental mapping images of Ni, Mn, and O.

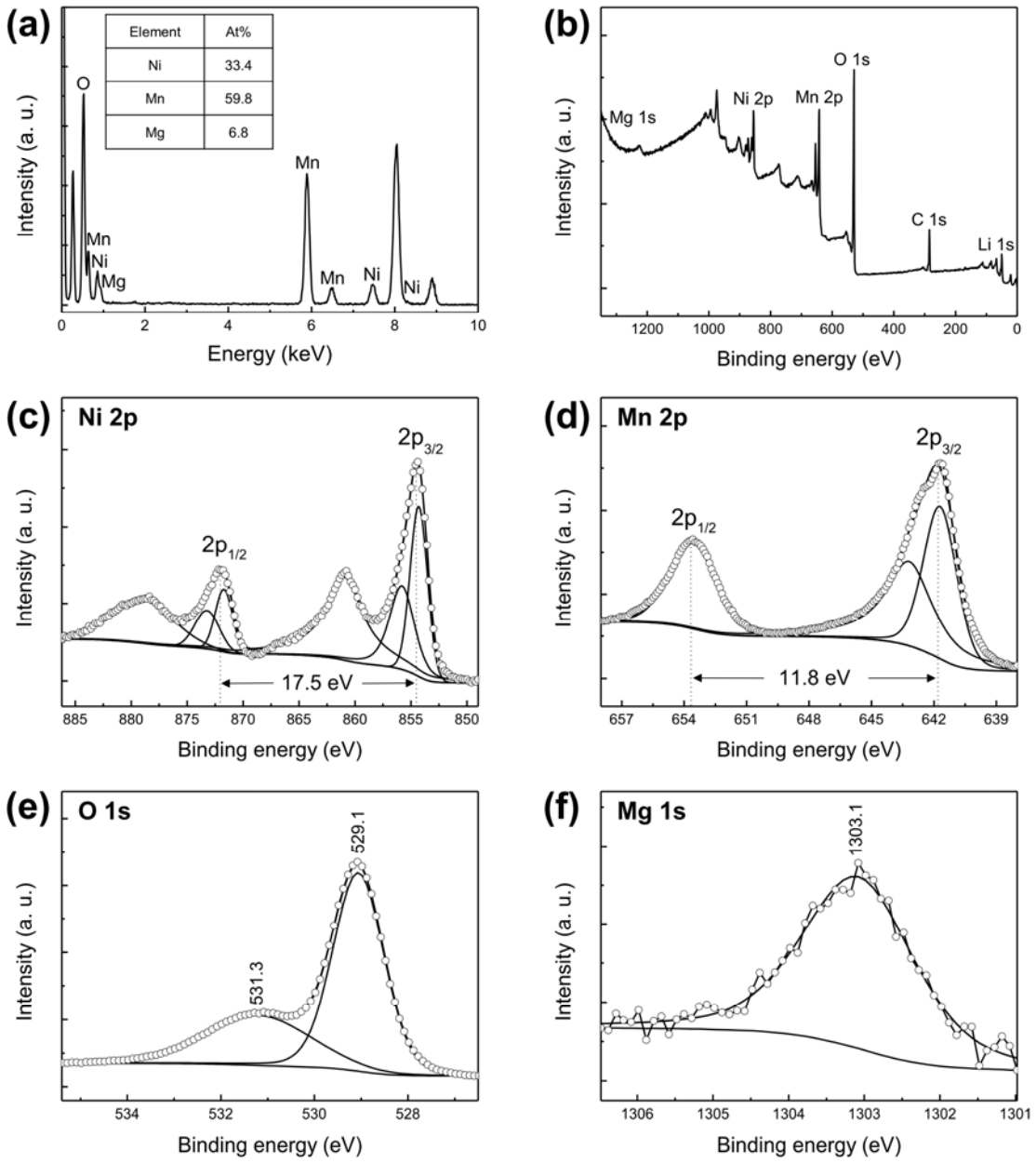

Fig. S3 (a) EDX spectrum of the LLNMO@Mg MSs. (b-f) XPS spectra of (b) full scan, (c) Ni 2p, (d) Mn 2p, (e) O 1s, (f) Mg 1s regions of the LLNMO@Mg MSs.

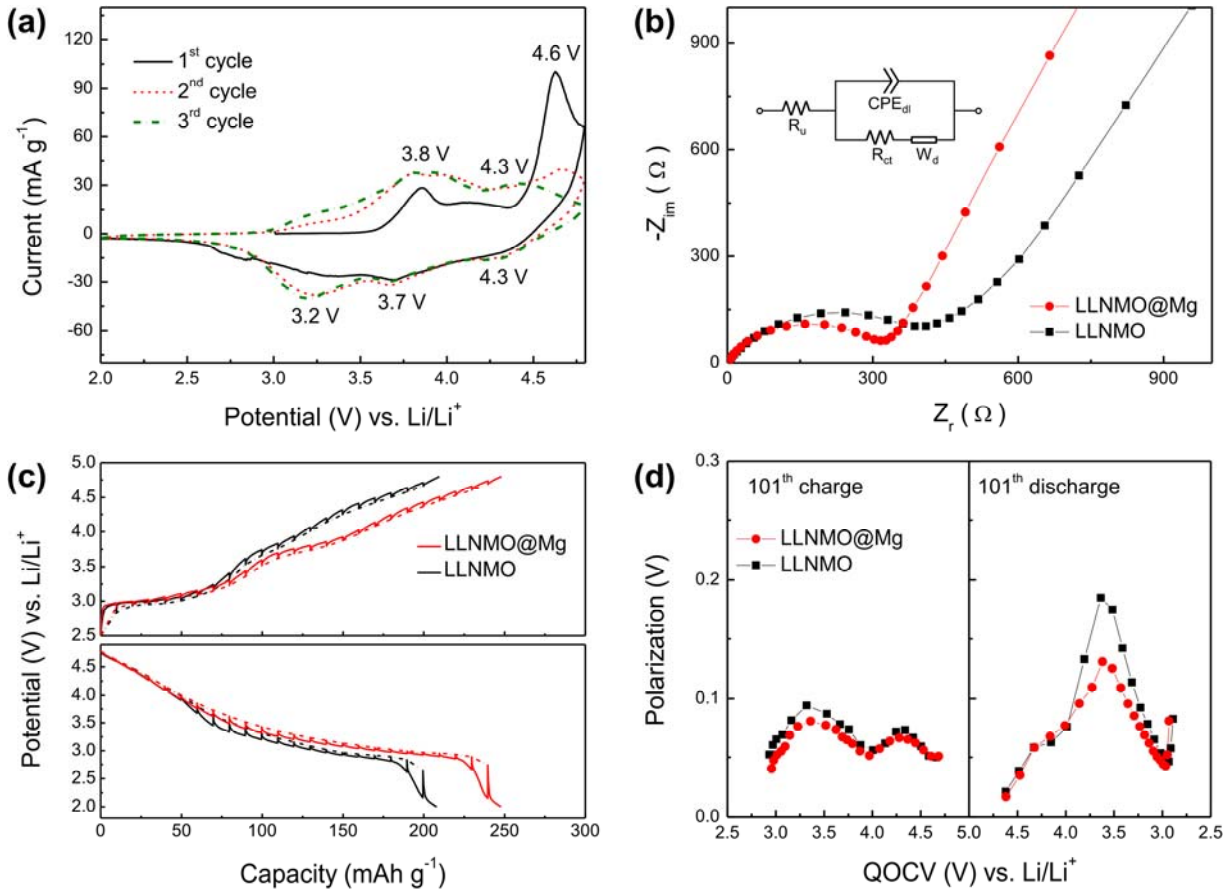

Fig. S4 (a) CVs of the LLNMO@Mg MSs between 4.8 and 2.0 V at a scan rate of 0.05 mV s^{-1}. (b) Nyquist plots of the LLNMO@Mg and LLNMO MSs measured at an open-circuit voltage of 2.0 V after the first cycle. Inset shows the equivalent circuit fitted with uncompensated resistance (R_u), charge transfer resistance (R_{ct}), double layer capacitance (CPE_{dl}), and Warburg impedance (W_d). (c) GITT curves of the LLNMO@Mg and LLNMO electrodes by 30 min charging/discharging and 1 h relaxation after the 100th cycle. (d) Polarization curves in the transient potential regions of the LLNMO@Mg and LLNMO MSs electrodes.

Fig. S4a shows the CV curves for the LLNMO@Mg MSs measured at a scan rate of 0.05 mV s^{-1} between 4.8 and 2.0 V, whose CV profiles are analogous to previously reported Li-rich cathode materials.[S1,S2] In the anodic sweep, two anodic peaks at 3.8 and 4.6 V were observed. The well-defined anodic peak at 3.8 V can be assigned to the Ni^{2+} oxidation to Ni^{4+}, while the peak at 4.3 V could be ascribed to the oxidation of Mn^{3+} to Mn^{4+}. The other sharp anodic peak at 4.6 V could be related to the Li_2MnO_3 activation. In the following cathodic sweep, the reduction peak at 3.7 V could be attributed to the Ni^{4+} reduction, while the peak at 3.2 V could be assigned to the Mn^{4+} reduction to Mn^{3+}.[S1,S2] Hence, the reversible redox reaction of the LLNMO@Mg MSs involved both Ni and Mn elements. The changes in the cycling profiles from the second cycle onward were quite smooth, indicating good cycling reversibility of the LLNMO@Mg MSs.

In order to understand the reasons for the enhanced performances of the LLNMO@Mg MSs, potential polarization curves were obtained from the GITT measurements after the 100^{th} cycle, as shown in Fig. S4c. The polarization curves were plotted by the difference between the closed-circuit and quasi-open-circuit potential in the transient potential profiles.[S3] The LLNMO@Mg MSs electrode shows a smaller polarization in Fig. S4d, which means that the LLNMO@Mg MSs could have enhanced charge transfer rates, compared with bare LLNMO MSs.[S4] Therefore, the Li^+ diffusivity of the LLNMO@Mg MSs could be definitely higher than that of the bare LLNMO MSs electrodes.

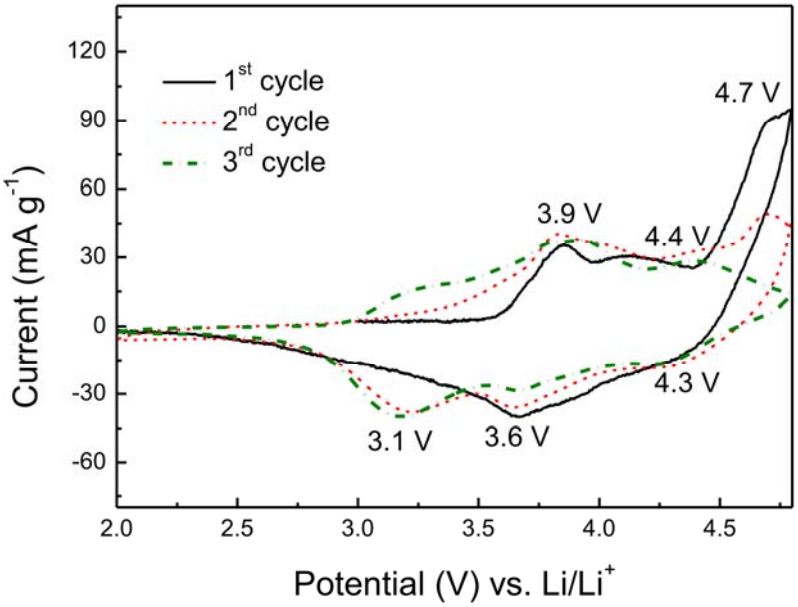

Fig. S5 CVs of the LLNMO MSs electrode from 4.8 to 2.0 V at a scan speed of 0.05 mV s^{-1}.

As shown in Fig. S5, the bare LLNMO MSs electrode showed large potential polarization compared with the LLNMO@Mg MSs, indicating that the LLNMO@Mg MSs could have improved kinetic properties.

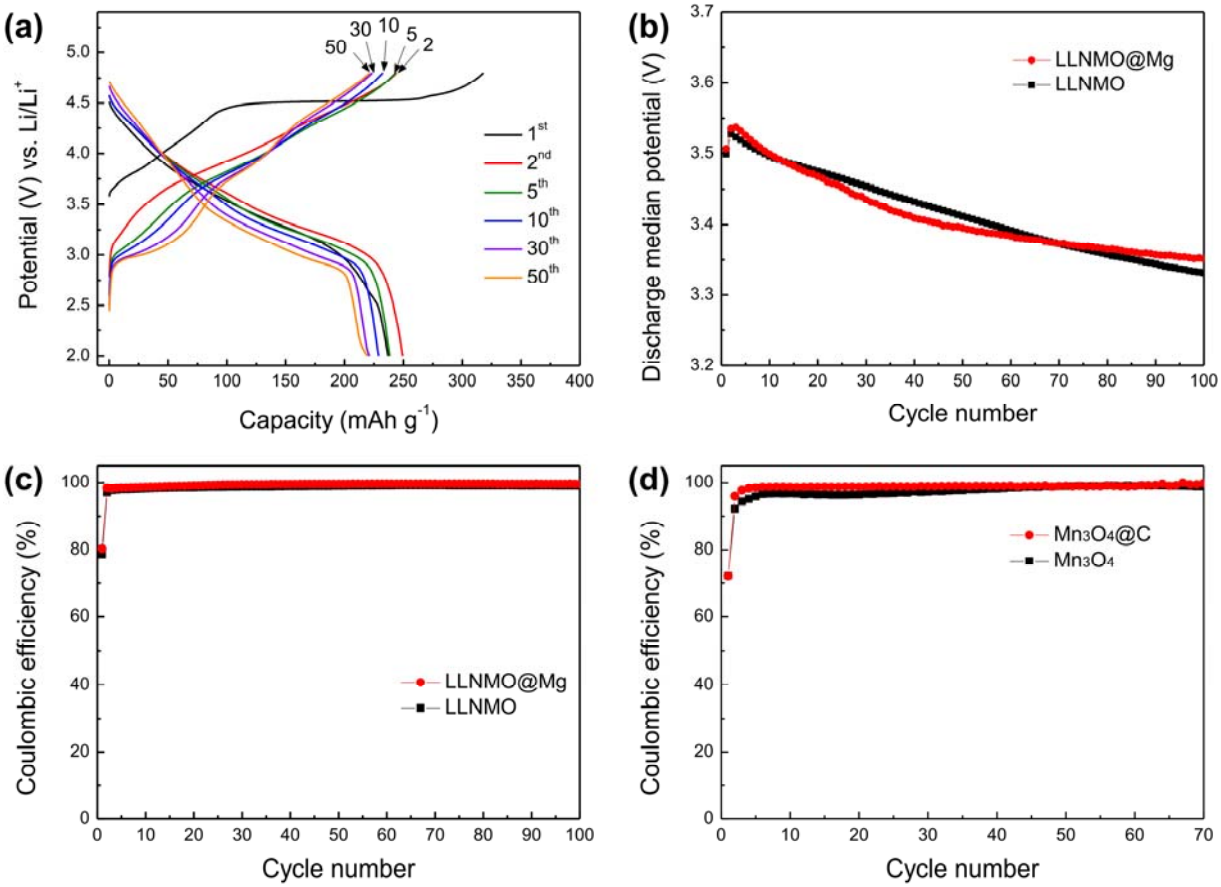

Fig. S6 (a) Potential profiles of the bare LLNMO MSs. (b) Discharge median potential profiles of the LLNMO@Mg and LLNMO MSs electrodes. Coulombic efficiency-cycle number curves of (c) LLNMO@Mg and (d) Mn_3O_4@C electrodes.

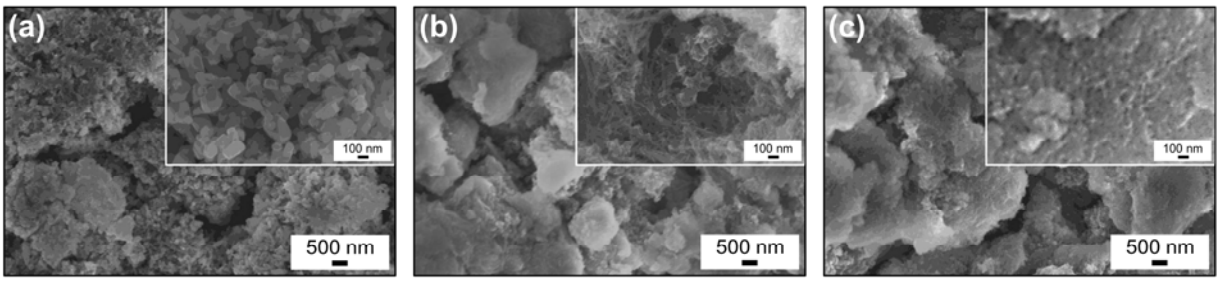

Fig. S7 (a-c) SEM images of (a) LLNMO@Mg, (b) Mn_3O_4@C, and (c) Mn_3O_4 MSs electrodes in the half-cell after cyclings.

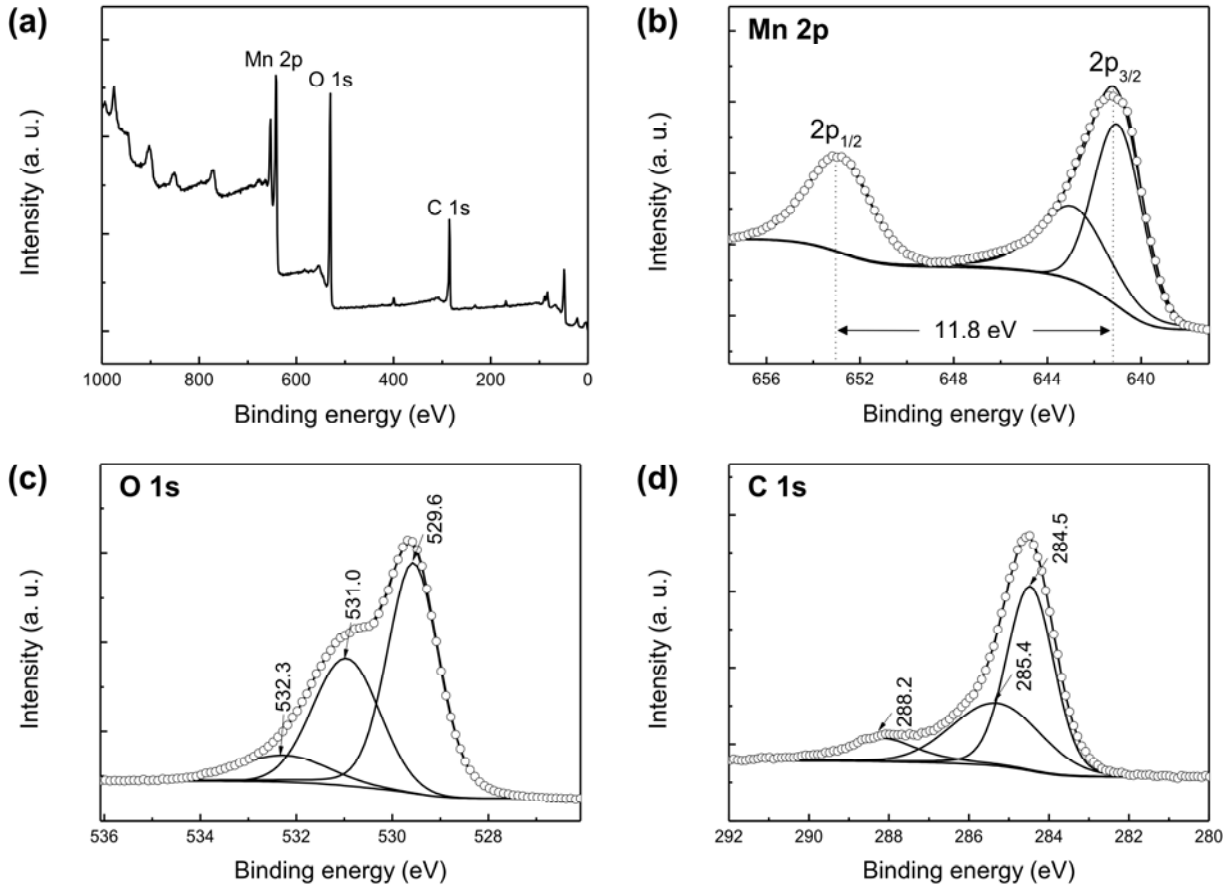

Fig. S8 (a-d) XPS spectra of (a) full scan, (b) Mn 2p, (c) O 1s, (d) C 1s regions of the Mn_3O_4@C MSs.

XPS analysis was performed to examine the oxidation state of Mn, O, and C elements in the Mn_3O_4@C MSs. The XPS survey spectra of the Mn_3O_4@C MSs are depicted in Fig. S8a. In Fig. S8b, the peaks at 653.1 and 641.3 eV can be attributed to Mn $2p_{1/2}$ and Mn $2p_{3/2}$, respectively. The binding energy difference is 11.8 eV, which is in line with previous reports.[S5,S6] As shown in Fig. S8c, the O 1s photoelectron peak is deconvoluted into three peaks: the main peak at 529.6

eV is ascribed to the oxygen species in the Mn_3O_4 MSs, while minor peaks at 531.0 and 532.3 eV correspond to the OH^- species or chemisorbed oxygen.[S5] As shown in Fig. S8d, the C 1s spectrum peaks can be resolved into three peaks: one peak at 284.5 eV is attributed to C–C, whereas the other peaks at 285.4 and 288.2 eV can be assigned to C–O, and C=O, respectively.[S6] Consequently, the XPS spectra further demonstrate that the Mn_3O_4@C MSs are composed of the Mn_3O_4 and carbon layers.

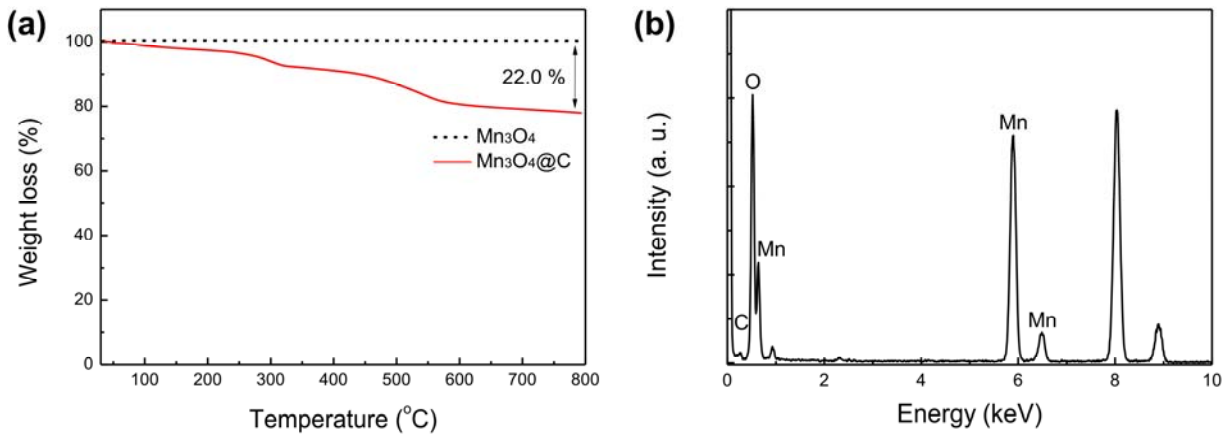

Fig. S9 (a) TGA curves of the Mn_3O_4@C and Mn_3O_4 MSs. (b) EDX spectrum of the Mn_3O_4@C MSs.

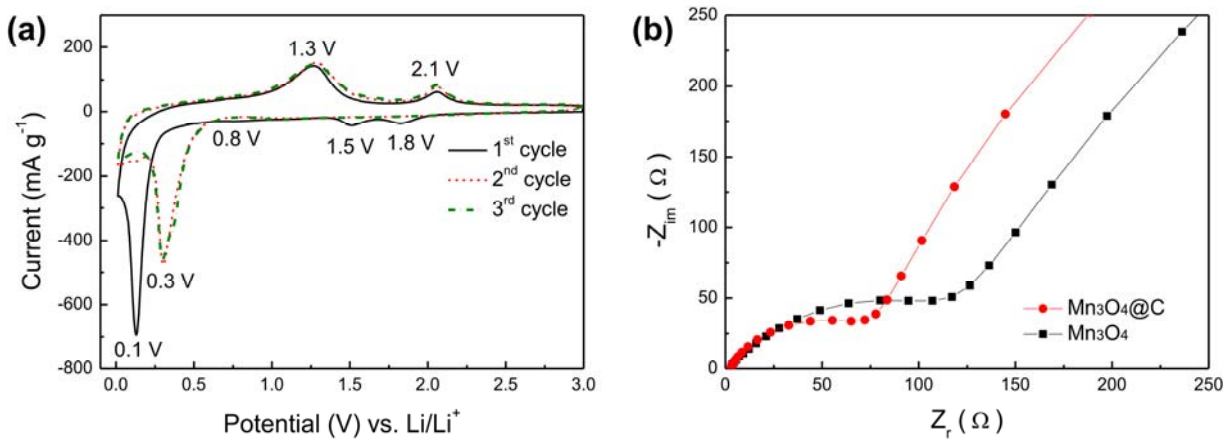

Fig. S10 (a) CV profiles of Mn_3O_4@C MSs at a scan rate of 0.05 mV s^{-1}. (b) Nyquist plots of the Mn_3O_4@C and Mn_3O_4 MSs measured at an open-circuit voltage of 3.0 V after the first cycle.

Fig. S10a presents the CV profiles for the Mn_3O_4@C MSs electrode obtained from 3.0 to 0.01 V at a scan rate of 0.05 mV s^{-1}, whose curves are analogous to previously reported Mn_3O_4-based materials.[S7,S8] In the first cycle, there are weak reduction peaks at 1.8 and 1.5 V, which are assigned to the compound formation of Li in Mn_3O_4 and reduction of Mn_3O_4 to MnO, respectively.[S7] The intense peak at 0.1 V is related to the MnO reduction to Mn^0. The broad peak at 0.8 V is attributed to the SEI layer formation. In the first oxidation process, the peaks at 1.3 and 2.1 V are observed, which are in accordance with the oxidation of metallic Mn^0 to MnO and oxidation of MnO to Mn_3O_4, respectively.[S7,S8] The CV profiles in the subsequent two cycles almost overlap, implying enhanced cyclability of the Mn_3O_4@C MSs electrode.

To further understand the enhanced electrode kinetics of the Mn_3O_4@C MSs as compared with the Mn_3O_4 MSs, the resistance was investigated with EIS measurements. A semicircle at a high-to-medium frequency and a sloping line at a low frequency were observed in the Nyquist

plots, as shown in Fig. S10b. From the Nyquist plots, the charge transfer resistance (R_{ct}) of the Mn_3O_4@C MSs electrode (72.1 Ω) is much smaller than that of the Mn_3O_4 electrode (107.1 Ω), indicating the improved electrical conductivity and Li^+ transfer rate by the carbon coating to the Mn_3O_4 MSs.[S3] Therefore, the Mn_3O_4@C MSs showed enhanced electrochemical properties compared to the bare Mn_3O_4 MSs electrode.

References

(S1) L. Li, L. Wang, X. Zhang, Q. Xue, L. Wei, F. Wu and R. Chen, *ACS Appl. Mater. Interfaces*, 2017, **9**, 1516-1523.

(S2) D. Chen, Q. Yu, X. Xiang, M. Chen, Z. Chen, S. Song, L. Xiong, Y. Liao, L. Xing and W. Li, *Electrochim. Acta*, 2015, **154**, 83-93.

(S3) J. G. Kim, Y. Noh and Y. Kim, *J. Ind. Eng. Chem.*, 2022, **107**, 280-290.

(S4) Y. J. Nam, D. Y. Oh, S. H. Jung and Y. S. Jung, *J. Power Sources*, 2018, **375**, 93-101.

(S5) W. Mao, W. Yue, Z. Xu, J. Wang, J. Zhang, D. Li, B. Zhang, S. Yang, K. Dai, G. Liu and G. Ai, *ACS Appl. Mater. Interfaces*, 2020, **12**, 39282-39292.

(S6) S.-C. Weng, S. Brahma, P.-C. Huang, Y.-C. Huang, Y.-H. Lee, C.-C. Chang and J.-L. Huang, *Appl. Surf. Sci.*, 2020, **505**, 144629.

(S7) Y. Qin, Z. Jiang, L. Guo, J. Huang and Z.-J. Jiang, *Chem. Eng. J.*, 2021, **406**, 126894.

(S8) D. Zhang, G. Li, J. Fan, B. Li and L. Li, *Chem. Eur. J.*, 2018, **24**, 9632-9638.